Infrared Physics & Technology 80 (2017) 120–130

Contents lists available at ScienceDirect

Infrared Physics & Technology

journal homepage: www.elsevier.com/locate/infrared

Long wavelength infrared radiation thermometry for non-contact temperature measurements in gas turbines

J. Manara [a,*], M. Zipf [a], T. Stark [a], M. Arduini [a], H.-P. Ebert [a], A. Tutschke [b], A. Hallam [c], J. Hanspal [c], M. Langley [c], D. Hodge [c], J. Hartmann [d]

[a] Bavarian Center for Applied Energy Research (ZAE Bayern), Magdalene-Schoch-Str. 3, 97074 Wuerzburg, Germany
[b] Siemens AG, Energy Sector, Fossil Power Generation Division, Huttenstr. 12, 10553 Berlin, Germany
[c] Meggitt Sensing Systems, The Laurels, Jays Close, Viables Industrial Estate, Basingstoke RG22 4BS, United Kingdom
[d] University of Applied Science Wuerzburg-Schweinfurt, Ignaz-Schön-Str. 11, 97421 Schweinfurt, Germany

HIGHLIGHTS

- Experimental setup for infrared-optical investigations at high temperatures.
- Infrared-optical characterisation of semi-transparent thermal barrier coatings.
- Development and validation of a long wavelength infrared radiation thermometer.
- Non-contact temperature measurement in gas turbine engines during operation.
- Uncertainty analysis of temperatures determined during engine test.

ARTICLE INFO

Article history:
Received 8 July 2016
Revised 25 November 2016
Accepted 25 November 2016
Available online 1 December 2016

Keywords:
Long wavelength infrared
Non-contact temperature measurement
Radiation thermometry
Thermal barrier coating
Emissivity
Gas turbine

ABSTRACT

The objective of the EU project "Sensors Towards Advanced Monitoring and Control of Gas Turbine Engines (acronym STARGATE)" is the development of a suite of advanced sensors, instrumentation and related systems in order to contribute to the developing of the next generation of green and efficient gas turbine engines. One work package of the project deals with the design and development of a long wavelength infrared (LWIR) radiation thermometer for the non-contact measurement of the surface temperature of thermal barrier coatings (TBCs) during the operation of gas turbine engines.

For opaque surfaces (e.g. metals or superalloys) radiation thermometers which are sensitive in the near or short wavelength infrared are used as state-of-the-art method for non-contact temperature measurements. But this is not suitable for oxide ceramic based TBCs (e.g. partially yttria stabilized zirconia) as oxide ceramics are semi-transparent in the near and short wavelength infrared spectral region. Fortunately the applied ceramic materials are non-transparent in the long wavelength infrared and additionally exhibit a high emittance in this wavelength region.

Therefore, a LWIR pyrometer can be used for non-contact temperature measurements of the surfaces of TBCs as such pyrometers overcome the described limitation of existing techniques. For performing non-contact temperature measurements in gas turbines one has to know the infrared-optical properties of the applied TBCs as well as of the hot combustion gas in order to properly analyse the measurement data. For reaching a low uncertainty on the one hand the emittance of the TBC should be high (>0.9) in order to reduce reflections from the hot surrounding and on the other hand the absorbance of the hot combustion gas should be low (<0.1) in order to decrease the influence of the gas on the measured signal.

This paper presents the results of the work performed by the authors with focus on the implementation of the LWIR pyrometer and the selection of the optimal wavelength band where the detector should be sensitive. Besides determining the spectral infrared-optical properties (emittance, transmittance and absorbance) of the TBCs and the hot combustion gas at high temperatures up to 1700 K, the wavelength specification of the developed LWIR pyrometer is defined. Also an overview of the LWIR radiation thermometer is given and the preliminary results for different temperatures and environmental conditions are presented. Finally the measurement uncertainty of the LWIR-pyrometer is deduced.

* Corresponding author.
E-mail address: jochen.manara@zae-bayern.de (J. Manara).

http://dx.doi.org/10.1016/j.infrared.2016.11.014
1350-4495/

1. Introduction

Turbine inlet temperatures of next generation gas turbines have to be increased in order to be thermodynamically more efficient [1]. To protect the metallic blades from these high temperatures and to guarantee long life, turbine blades usually use a Thermal Barrier Coating (TBC) [2]. Detailed knowledge of the turbine blade and TBC temperature is critical to evaluate the effectiveness of cooling designs as well as to identify problematic blades during service [3]. Conventional short wavelength pyrometry (around 1 μm) [4] is not suitable due to substantial errors caused by the optical transparency of the TBC at these wavelengths [5–7], so longer wavelengths are required (around 10 μm) where the TBC is effectively opaque and its temperature can be measured directly [8].

Metallic turbine blades at the first two or three turbine stages are coated with ceramic heat shields (i.e. TBCs) to protect them from high combustion gas temperature load and also to ensure long lifetime of the blades. These ceramic thermal barrier coatings are usually made of a 200–500 μm thick partially yttria-stabilized zirconia (PYSZ). New TBCs have a clean white or yellowish colour that changes during operation in the engine with time under thermal load to a brownish and/or reddish brown colour. The colour change results from deposits that are present in the gas flow, mainly on the pressure side and leading edge of a blade. These deposits contain the metallic elements Ti, Fe and Ni certainly originating from debris of metallic turbine components. Depending on the geographical region where an engine is used, the deposits also contain a number of molten calcium-magnesium-alumino-silicates (CMAS) resulting from dust, sand and ash [9].

All of the parameters given above influence the optical and infrared-optical characteristics of the TBCs and thus the obtainable precision of a pyrometer measurement.

Therefore a set of specimens of free standing PYSZ-TBCs have been investigated which included clean, white TBCs as well as TBCs with different degrees of colouring due to deposit fouling. The artificial deposits on the TBC which simulates the observed changes during operation are mainly Fe_3O_4, FeO-Fe_2O_3 and partly Fe_2O_3, giving a good representation of real engine deposits originating from metallic engine parts.

Additionally the infrared-optical properties of the hot gas have been analysed, which mainly comprises nitrogen and oxygen as well as carbon dioxide and water vapour as infrared-active gases.

Based on these data the optimum wavelength range for the LWIR radiation thermometry has been chosen and a LWIR pyrometer setup has been developed.

The choice of operating wavelength ranges of this LWIR-pyrometer setup depended primarily on two factors which are:

- The spectral emittance and transmittance profile of the TBCs:
  Optimally the TBCs should provide a high emittance and a vanishing transmittance at the given wavelengths.
- The spectral transmittance and absorptance of the hot gas in the optical path between the pyrometer and the turbine:
  Optimally the hot gas should provide a high transmittance at the required wavelengths, a low absorptance and low emission.

The final LWIR-pyrometer design contains many elements from an existing short-wavelength pyrometer design. This comprises a mirror and lens system to collect radiation from a defined spot on the blade and focus it onto an optical fibre, which then relays the radiation signal to a remote photo-detector for analysis. The design methodology adopted was to work towards the final design in three stages, as follows:

- Laboratory testing of likely designs using 'off the shelf' (OTS) optical components and mounting fixtures.
- A 'benchtop' version which uses customised lenses and mountings that are dimensionally compatible with the short-wavelength pyrometer.
- Final prototype using customised lenses and mountings that can be assembled into the body of the short-wave pyrometer for testing on the engine.

In Section 2 the experimental setups are described which have been used for characterising the TBCs and the hot combustion gas. In this work the thermal barrier coatings have been investigated from ambient up to high temperatures.

The characteristics of the investigated TBCs and the hot gas are given in Section 3. The design of the LWIR-pyrometer based on these results is introduced in Section 4 together with the test measurements in the laboratory and at the test rig.

2. Experimental setup

2.1. Infrared-optical characterisation at room temperature

At ambient temperature an integrating sphere apparatus can be used for measuring the spectral directional-hemispherical reflectance R_{dh} and transmittance T_{dh} of the specimens (Fig. 1). The directional spectral emittance ε_λ normal to the surface is than calculated from the spectral directional-hemispherical reflectance R_{dh} and transmittance T_{dh} [10,11]:

$$\varepsilon_\lambda = 1 - R_{dh} - T_{dh}. \quad (1)$$

The specimens were measured with a FTIR-spectrometer (IFS Vertex 70v from Bruker) in the wavelength range between 2 μm and 18 μm.

2.2. Infrared-optical characterisation at high temperatures

The black-body boundary conditions (BBC) apparatus allows determining the directional spectral emittance as well as the directional-hemispherical spectral transmittance and reflectance normal to the specimen surface as a function of temperature [7,12]. By changing the boundary conditions of the specimen it is possible to obtain the desired quantities. In front of and behind the specimen, so called black-body surroundings with an emittance close to unity and variable temperatures, allow generating different boundary conditions. Fig. 2 shows the four configurations used. The black-body surroundings have a temperature T_b or T_u, where $T_b > T_u$. The specimen is heated in a furnace to a temperature T with $T > T_b$. It is then quickly positioned in the beam path and measurements made.

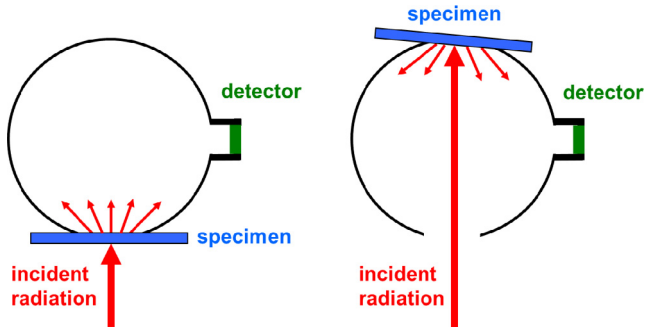

Fig. 1. Measurement of the directional-hemispherical transmittance T_{dh} (on the left side) and the directional-hemispherical reflectance R_{dh} (on the right side) using an integrating sphere.

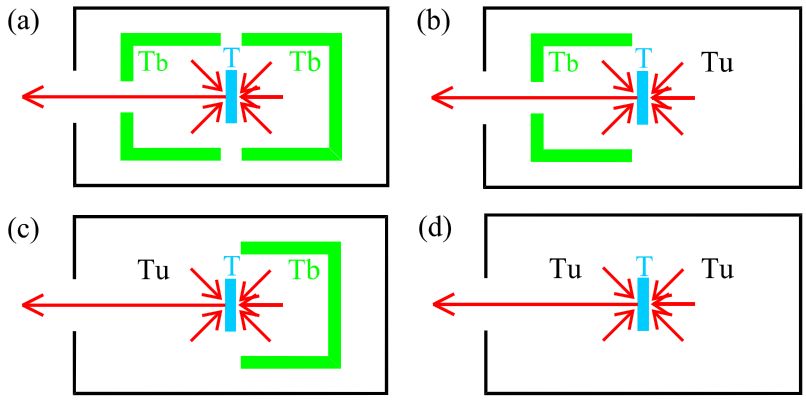

Fig. 2. Black-body boundary conditions (BBC) method with different boundary conditions to determine the directional spectral emittance as well as the directional-hemispherical spectral transmittance and reflectance.

In Fig. 2a the black-body surroundings in front of and behind the specimen have the same temperature T_b. The detected intensity I_{meas} (long arrow) is given by:

- intensity, emitted by the specimen itself: $\varepsilon_\lambda(T) \cdot I_b(\lambda, T)$,
- intensity, impinging the specimen from the front half space and reflected by the specimen itself: $R_{gh}(T) \cdot I_b(\lambda, T_b)$,
- intensity, impinging the specimen from the back half space and transmitted by the specimen itself: $T_{gh}(T) \cdot I_b(\lambda, T_b)$,

i.e.:

$$I_{meas}(\lambda, T, T_b) = \varepsilon_\lambda(T) \cdot I_b(\lambda, T) + [R_{gh}(T) + T_{gh}(T)] \cdot I_b(\lambda, T_b). \quad (2)$$

Using Eq. (1) and solving Eq. (2) for the spectral emittance yields:

$$\varepsilon_\lambda(T) = \frac{I_{meas}(\lambda, T, T_b) - I_b(\lambda, T_b)}{I_b(\lambda, T) - I_b(\lambda, T_b)}. \quad (3)$$

The cases in Fig. 2a and d are the same, only the temperature of the black-body surroundings are different. The detected intensity in Fig. 2d is:

$$I_{meas}(\lambda, T, T_u) = \varepsilon_\lambda(T) \cdot I_b(\lambda, T) + [R_{gh}(T) + T_{gh}(T)] \cdot I_b(\lambda, T_u). \quad (4)$$

For the configuration in Fig. 2d the emittance is:

$$\varepsilon_\lambda(T) = \frac{I_{meas}(\lambda, T, T_u) - I_b(\lambda, T_u)}{I_b(\lambda, T) - I_b(\lambda, T_u)}. \quad (5)$$

With configuration Fig. 2b and c it is possible to measure the directional-hemispherical spectral transmittance and reflectance. Together with the case in Fig. 2a or d three measurements are performed to determine the three quantities emittance, reflectance and transmittance. The measured intensity in Fig. 2b, analogously to the measured intensity in Fig. 2a, is given by:

$$I_{meas}(\lambda, T, T_b, T_u) = \varepsilon_\lambda(T) \cdot I_b(\lambda, T) + R_{gh}(T) \cdot I_b(\lambda, T_b) + T_{gh}(T) \cdot I_b(\lambda, T_u). \quad (6)$$

The same is valid for the configuration in Fig. 2c:

$$I_{meas}(\lambda, T, T_u, T_b) = \varepsilon_\lambda(T) \cdot I_b(\lambda, T) + R_{gh}(T) \cdot I_b(\lambda, T_u) + T_{gh}(T) \cdot I_b(\lambda, T_b). \quad (7)$$

Subtracting Eq. (6) from Eq. (2) one obtains the spectral directional-hemispherical transmittance as function of two measured spectra and two theoretical black-body spectra at the temperatures T_b and T_u:

$$T_{gh}(T) = \frac{I_{meas}(\lambda, T, T_b) - I_{meas}(\lambda, T, T_b, T_u)}{I_b(\lambda, T_b) - I_b(\lambda, T_u)}. \quad (8)$$

The spectral directional-hemispherical reflectance is obtained analogously by subtracting Eq. (7) from Eq. (2):

$$R_{gh}(T) = \frac{I_{meas}(\lambda, T, T_b) - I_{meas}(\lambda, T, T_u, T_b)}{I_b(\lambda, T_b) - I_b(\lambda, T_u)}. \quad (9)$$

Beside the normal emittance (= directional emittance perpendicular to the surface), the directional emittance can also be measured as a function of the emission angle. This has been done by a so called emittance measurement apparatus (EMMA). With the EMMA-setup measurements can be performed at different emission angles as a function of wavelength λ and temperature T [13,14].

For this purpose again the radiation from the surroundings, which is irradiated onto the specimen and reflected by the specimen has to be taken into account.

The intensity i_{meas} coming from the specimen consists of the intensity emitted by the specimen itself and the intensity from the black surrounding which is reflected by the specimen into the considered direction:

$$i_{meas}(\lambda, T_{sp}) = \varepsilon_\lambda(T_{sp}) \cdot i_b(\lambda, T_{sp}) + [1 - \varepsilon_\lambda(T_{sp})] \cdot i_b(\lambda, T_a), \quad (10)$$

with $i_b(\lambda, T_{sp})$ = intensity emitted by a black body at the temperature T_{sp}, $i_b(\lambda, T_a)$ = intensity emitted from the black surrounding at ambient temperature T_a.

Solving Eq. (10) gives the spectral emittance ε_λ as

$$\varepsilon_\lambda(T_{sp}) = \frac{i_{meas}(\lambda, T_{sp}) - i_b(\lambda, T_a)}{i_b(\lambda, T_{sp}) - i_b(\lambda, T_a)}. \quad (11)$$

A scheme of the measurement setup can be found in Fig. 3. For the measurements, the specimen is mounted onto the top side of a furnace. The black enclosure is coated with Nextel Velvet Coating which has an emittance of 0.98 and is cooled by a thermostat to a uniform temperature T_a of 300 K. For measuring the emittance as a function of the emission angle the furnace can be rotated as illustrated in Fig. 3.

2.3. Infrared-optical characterisation of hot gases

To determine the influence of the combustion gases, a measurement set-up was used, which is schematically illustrated in Fig. 4. As radiation source, a black body or a TBC-specimen is used, heated to a defined temperature. The gas with customised composition is placed in front of the radiation source inside a high-pressure cell at defined temperature and pressure. The transmitted radiation is measured by a Fourier transform infrared spectrometer.

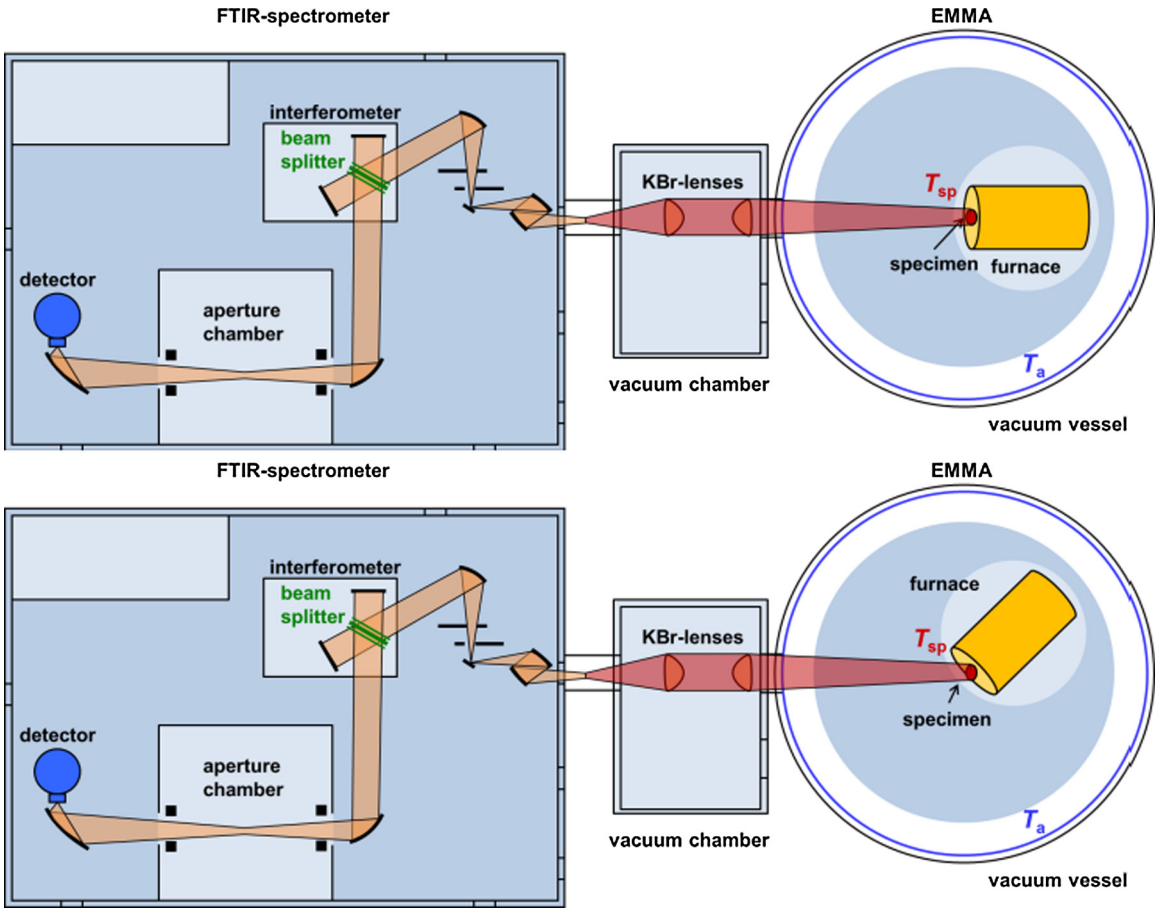

Fig. 3. Measurement setup for determining the directional spectral emittance at high temperatures. Top: Measurement of the directional emittance normal to the surface (= normal emittance). Bottom: Measurement of the directional emittance at different emission angles between 0° and 70°.

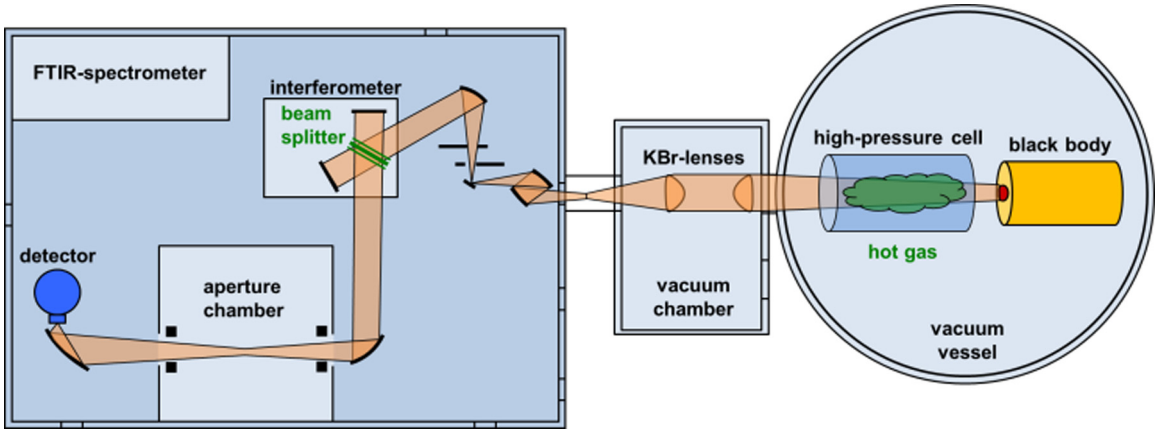

Fig. 4. Schematic illustration of the setup for determining the influence of the hot gas between the TBC and the detector using a FTIR-spectrometer and a high-pressure cell.

3. Results and discussion

3.1. TBC characteristics

A set of free standing TBCs with different thicknesses between 150 µm and 500 µm based on partially yttria stabilized zirconia (PYSZ) were prepared by atmospheric plasma spraying (APS) on a substrate and separating the TBC layer afterwards. Additionally these free standing TBC layers were artificially aged by depositing Fe_3O_4, FeO-Fe_2O_3 and partly Fe_2O_3 and other compounds containing Ti, Fe and Ni as well as calcium-magnesium-alumino-silicates (CMAS).

New PYSZ-TBCs have a clean white or yellowish color that changes in the engine with time of thermal load to a brownish and/or reddish brown color. The color change results from deposits that are present mainly on the pressure side and leading edge of a blade. These deposits contain of metallic elements Ti, Fe, Ni certainly originating from debris of metallic turbine components. Depending on the region where the engine is used, the deposits also contain a more or less large number of molten calcium-magne

sium-alumino-selicates (CMAS) resulting from dust, sand and ash [15,16]. The artificially created deposits on the free-standing TBC is mainly Fe_3O_4 and FeO-Fe_2O_3 and partly Fe_2O_3 made of a solution of magnetite powder which contains iron(II,III) oxide. The free-standing TBC sample have been painted with the magnetite solution and heat treated afterwards at 1250 °C in air. Beside these samples another set of samples have been painted with a Fe-rich CMAS representing solution whose mixture corresponds to real land based heavy duty gas turbine CMAS compositions.

At first the TBCs were characterised at ambient temperature using the integrating sphere setup, and thereafter, at high temperatures using the black-body boundary conditions (BBC) apparatus. The resulting spectral transmittance of a free standing PYSZ-TBC with a thickness of 500 µm (specimen 1) is depicted in Fig. 5 for several temperatures. From Fig. 5 it can be seen that a significant transmittance occurs for wavelengths below 8 µm which decreases with increasing temperature. Nevertheless the transmittance is still considerably above zero in the near infrared (NIR), the short wavelength infrared (SWIR) and partially even in the mid infrared (MIR). Hence these wavelength regions are not suitable for a contactless determination of the surface temperature as not only radiation from the surface reaches the detector but also radiation from inside the TBC and even from the substrate. This leads to a false temperature reading.

Fortunately the transmittance vanishes for wavelengths above 8 µm and therefore the TBCs are opaque in the long wavelength infrared (LWIR). Thus the fundamental requirement for the usage of a LWIR-pyrometer is fulfilled as only radiation from the surface can reach the detector which offers the possibility for a non-contact determination of the surface temperature.

The spectral emittance of specimen 1 is shown in Fig. 6 at the same temperatures as in Fig. 5. The emittance increases with increasing temperature. Besides this the emittance at a temperature of 1300 K is above 0.9 for wavelengths between 8 µm and 18 µm and above 0.98 in the spectral region from 10 µm to 14 µm. At 13 µm, the so called Christiansen-wavelength [8], the spectral emittance equals unity [17]. A high emittance and a vanishing transmittance result in a low reflectance according to Eq. (1). Therefore the influence of the surrounding is relatively small as only a low amount of radiation from the hot surrounding is reflected by the TBC.

Following these explanations, the most suitable wavelength for non-contact measurement of PYSZ in the LWIR would be the Christiansen-wavelength at 13 µm. Unfortunately the hot combustion gas has an absorption band around 13 µm as discussed

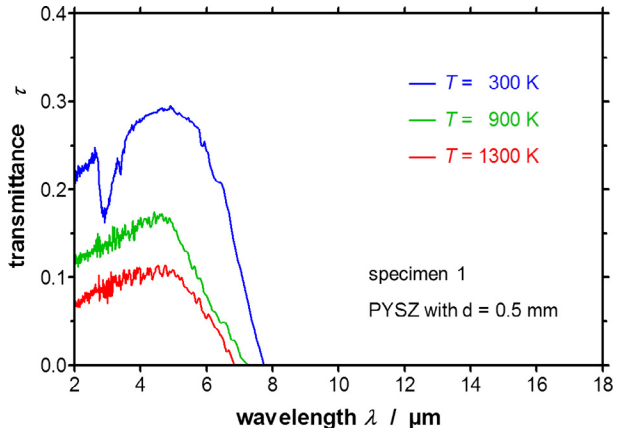

Fig. 5. Normal transmittance of PYSZ with a thickness of 0.5 mm for wavelengths between 2 µm and 18 µm at different temperatures ranging from 300 K to 1300 K.

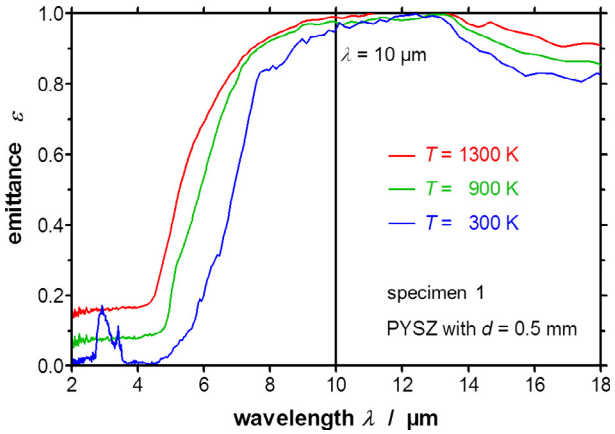

Fig. 6. Normal emittance of PYSZ with a thickness of 0.5 mm for wavelengths between 2 µm and 18 µm at different temperatures ranging from 300 K to 1300 K.

in Section 3.2. Hence 10 µm has been chosen as the appropriate wavelength with an emittance above 0.98.

Further investigations have been made using the emittance measurement apparatus (EMMA) in order to check the dependence of the emittance on the emission angle as well as on the fouling of the surface. In Fig. 7 the directional spectral emittance of a PYSZ-TBC with a thickness of 0.5 mm (specimen 7) is displayed for different emission angles relative to the surface normal at a temperature of 1300 K. The directional emittance does not change considerably with increasing angle up to an emission angle of 60°. A significant decrease of the emittance is only visible for larger angles above 60° (e.g. 70°). Therefore using a LWIR-pyrometer allows different viewing angles without critically influencing the emittance and consequently the deduced temperature, which is required for scanning curved surfaces such as turbine blades.

Furthermore the spectral emittance of three specimens, 1 (new specimen), 2 and 3 (differently aged specimens, resulting in varying amounts of fouling) has been determined at a temperature of 1300 K and the derived values are plotted in Fig. 8. The specimens with the letters A and B are each identical and provide the same emittance. Hence only one curve is given for each type of specimen (1, 2 and 3). Although the colours of the TBCs are remarkably different, the emittance in the LWIR around 10 µm is similar. This means that deposited compounds on the TBC are also of high emissivity around 10 µm. The emittance at other wavelengths (mainly

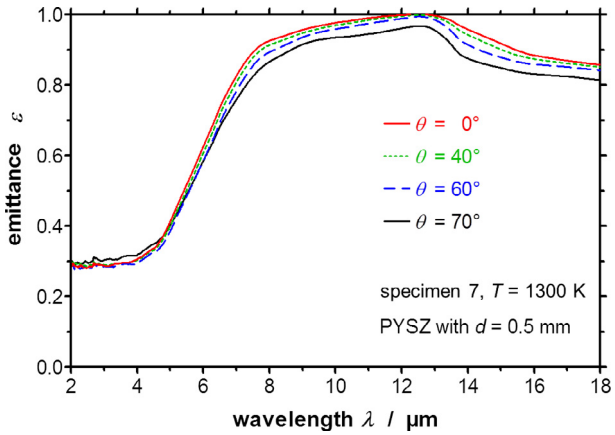

Fig. 7. Directional spectral emittance of PYSZ with a thickness of 0.5 mm in the wavelength range between 2 µm and 18 µm for different emissions angles from 0° (normal to the surface) and 70°.

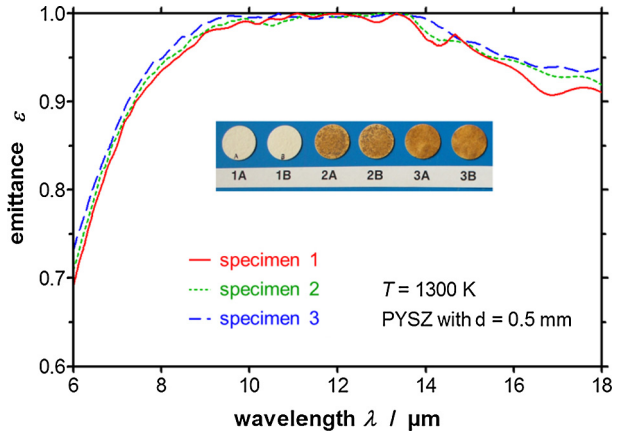

Fig. 8. Normal spectral emittance of PYSZ specimens with different amounts of fouling (specimen 1, 2 and 3) and a thickness of 0.5 mm in the wavelengths between 6 µm and 18 µm.

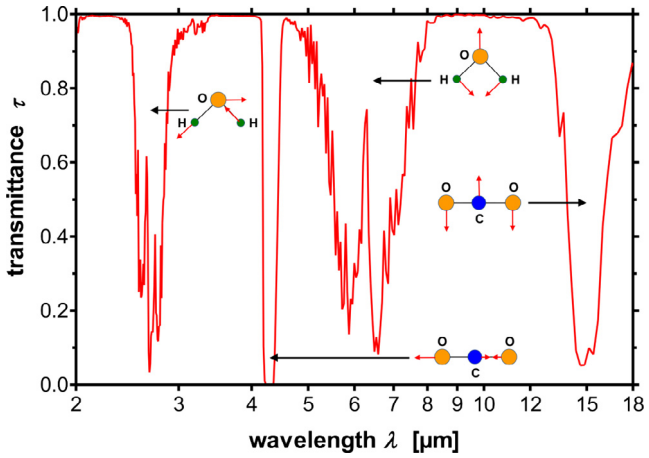

Fig. 9. Typical spectral transmittance of the water vapour and carbon dioxide in the wavelength range between 2 µm and 18 µm.

in the visible and near infrared spectral regions) may change significantly, but these wavelength regions are not the subject to this work. This leads to the desirable outcome that the non-contact temperature measurement with an LWIR-pyrometer is almost independent of the aging of the TBC and can therefore be used during the whole lifetime of the turbine blade without additional lifetime-dependent corrections of the detected signal.

3.2. Hot gas characteristics

The hot combustion gas mainly consists of nitrogen, oxygen, water vapour and carbon dioxide (see a usual composition in Table 1), where water vapour and carbon dioxide are infrared active. A typical temperature for the investigated turbine is 1600 K with a pressure of 13 bar. The resulting spectral transmittance of water vapour and carbon dioxide which has been measured at ZAE Bayern is plotted in Fig. 9. The molecules and corresponding oscillations are correlated with the respective absorption peaks in Fig. 9 [18]. It can be seen that around 10 µm a high transmittance occurs which enables a non-contact temperature measurement in this wavelength region. Therefore a filter with a high transmittance around 10 µm has been chosen for the LWIR-pyrometer setup.

First measurements with the apparatus described in Section 2.3 have been performed which confirm the transmittance given in Fig. 9. For a further validation additional measurements need to be made which will be reported in future publications.

Up to now it can be stated that a wavelength region around 10 µm is well suited for non-contact measurements of TBCs in gas turbines.

Table 1
Composition of the hot combustion gas in the investigated turbine at a temperature of 1600 K and a pressure of 13 bar.

gas	fraction
N_2	75 %
O_2	10 %
H_2O	10 %
CO_2	5 %

4. LWIR pyrometer setup and tests

4.1. LWIR benchtop pyrometer for laboratory tests

In Section 3, the radiation emitted by the TBC has been measured with a FTIR-spectrometer and the emittance of the TBC has been derived as described in Section 2. In this section measurements of the surface temperature of the TBC have been performed using a LWIR-pyrometer and a NIR-pyrometer in order to validate the theoretically expected physical correlations. For this purpose a free-standing PYSZ-TBC has been mounted on top of a furnace which heats the specimen to the desired temperature. The radiation emitted by the surface was measured at the same time with a LWIR-pyrometer at 10 µm and a NIR-pyrometer at 1 µm as depicted in Fig. 10. The temperature of the TBC was additionally measured using on the one hand a FTIR-spectrometer and the Christiansen-wavelength where the emittance equals [19] unity and on the other hand a thermocouple [4]. The derived temperatures are shown in Fig. 11 for a cold surrounding in front of the specimen and in Fig. 12 for a hot surrounding in front of the specimen. The investigated PYSZ-specimen exhibits an emittance of 0.98 at 10 µm and 0.30 at 1 µm. In Fig. 11 the analysis of the measured intensity has been additionally made for different (wrong) emittances in order to check its influence on the derived temperature.

The surface temperature measured with the LWIR-pyrometer and the correct emittance of 0.98 is in a good agreement with the temperature derived by the FTIR-spectrometer and the thermocouple. Furthermore the temperature derived from the LWIR-measurement varies with varying emittance of the surface as theoretically expected. The apparent temperature increases with decreasing emittance and vice versa. In contrast to that a significantly different temperature has been derived by the NIR-pyrometer. This is caused by the semi-transparency of the specimen around 1 µm and the fact that the specimen is heated from the back side which results in a temperature gradient from the back side to the front side. Hence a higher amount of radiation is detected by the NIR-pyrometer which partially comes from the backside of the specimen. Finally a higher apparent temperature is derived even if different emittances are chosen for data analysis.

In total, the apparent temperature of a PYSZ-TBC derived from the NIR-pyrometer lies more than 100 K above the correct surface temperature derived from the LWIR-pyrometer whereas the temperature derived from the LWIR-pyrometer equals the temperature derived by a thermocouple and the reference measurement with a

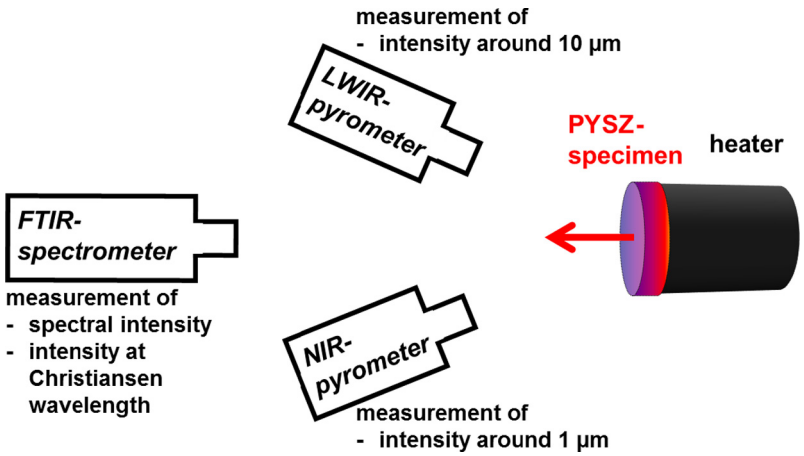

Fig. 10. Determination of the radiation emitted by a PYSZ-specimen with a FTIR-spectrometer, a LWIR-pyrometer and a NIR-pyrometer.

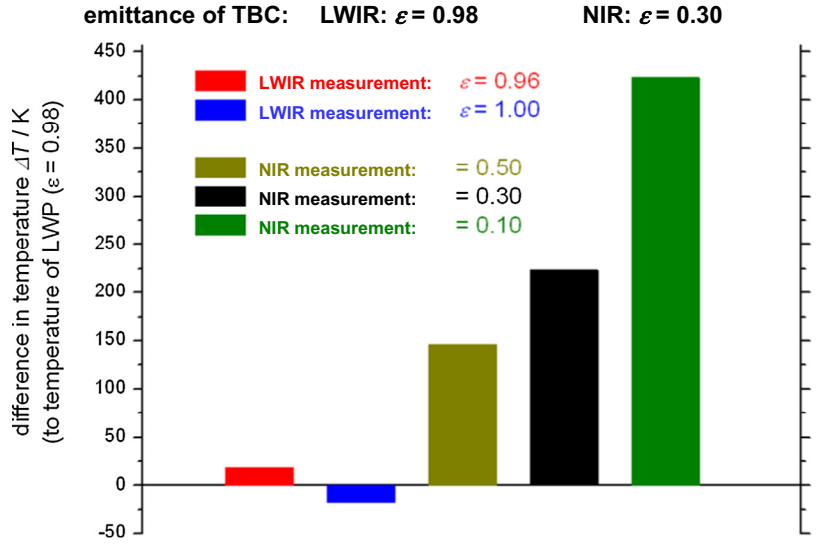

Fig. 11. Sensitivity analysis: Temperatures of a PYSZ-specimen derived from a LWIR- and a NIR-pyrometer for different assumed emittances of the surface (the actual emittances are given above the graph). The plotted values are the difference between the derived temperature and the actual temperature of the PYSZ-specimen, determined using Christianson wavelength.

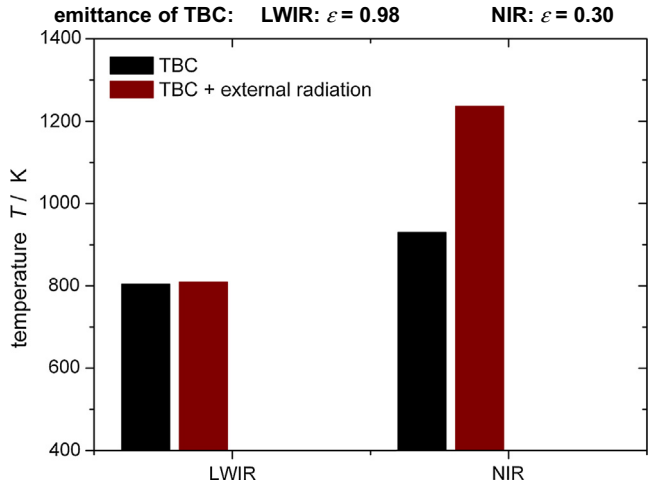

Fig. 12. Temperatures of a PYSZ-specimen derived from a LWIR- and a NIR-pyrometer for cold and hot surroundings (without and with external radiation) without an additional correction for the reflected radiation.

FTIR-spectrometer using the Christiansen-wavelength for temperature determination. Therefore a LWIR-pyrometer is well suited for determining the surface temperature of TBCs based on oxide ceramics.

Had the sample been heated from the front side with a temperature gradient from the warmer front side to the colder back side a lower temperature reading would be expected from the NIR-pyrometer compared to the LWIR-pyrometer.

The measurements were repeated for a hot surrounding in order to check the influence of radiation which is reflected by the surface of the TBC and then hits the detector. For visualisation of the effect, the apparent temperature without additional correction of the reflected radiation is depicted in Fig. 12. Obviously the detected radiation increases and thus the apparent temperature increases. In the LWIR only a slight increase is detectable due to the high emittance in this wavelength region whereas in the NIR a substantially larger increase occurs due to the low emittance at shorter wavelength. Of course the influence of reflected radiation can be corrected in order to derive the real surface temperature. But this requires, besides the knowledge of the emittance, exact knowledge of the surrounding condition, in particular the temperature, which is usually known only imprecisely during operation of

gas turbines. Therefore it is advantageous that the hot surrounding influences the LWIR-measurement only slightly as it significantly reduces the measurement uncertainty compared to the NIR-measurement.

Based on the above investigations, a LWIR-pyrometer has been developed in this project, which uses the principle setup of an existing NIR-pyrometer with adapted parts, such as infrared-transparent lenses and fibres as well as LWIR-filters and detectors. A scheme of the benchtop LWIR-pyrometer setup used for test measurements in the laboratory is shown in Fig. 13. This benchtop pyrometer contains ZnSe-lenses and apertures in order to guide the radiation from a defined spot on the TBC surface into the IR-fibre (core material $AgCl_{0.25}Br_{0.75}$ and cladding material $AgCl_{0.50}Br_{0.50}$) and via a coupler onto the liquid nitrogen cooled MCT-detector (mercury cadmium telluride-detector). In front of the detector different IR-filters can be placed. As explained above, a filter which transmits around 10 μm has been chosen.

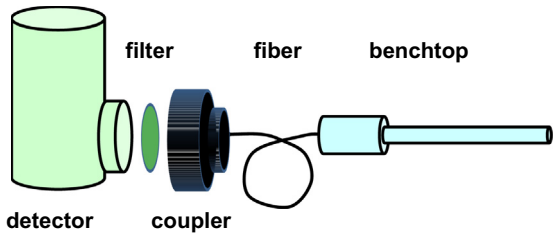

Fig. 13. Scheme of the benchtop LWIR-pyrometer setup.

4.2. LWIR-pyrometer for test facility measurements

Furthermore, a prototype has been developed for the test measurements at the Siemens Berlin test facility (BTF) which consists of a lance (Fig. 14) instead of the benchtop pyrometer. Here the detector is mounted in a separate box (Fig. 16) for thermal and electrical insulation. Besides ZnSe-lenses and an aperture the lance includes a gold mirror in order to redirect the radiation from a TBC coated turbine blade into the lance and thence into the fibre. Water cooling and nitrogen purge prevent overheating and fouling of the mirror and the first lens, respectively. The radiation is then guided through the fibre onto the MCT-detector after having passed

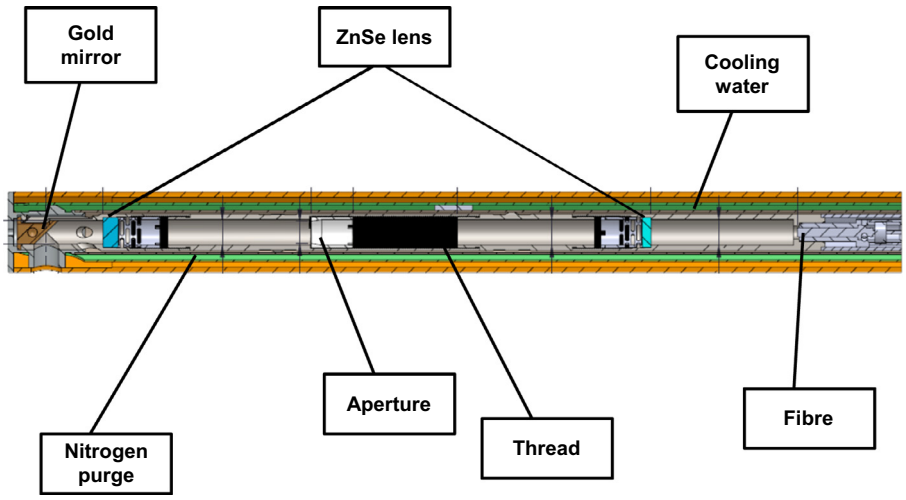

Fig. 14. Prototype of pyrometer lance for engine testing.

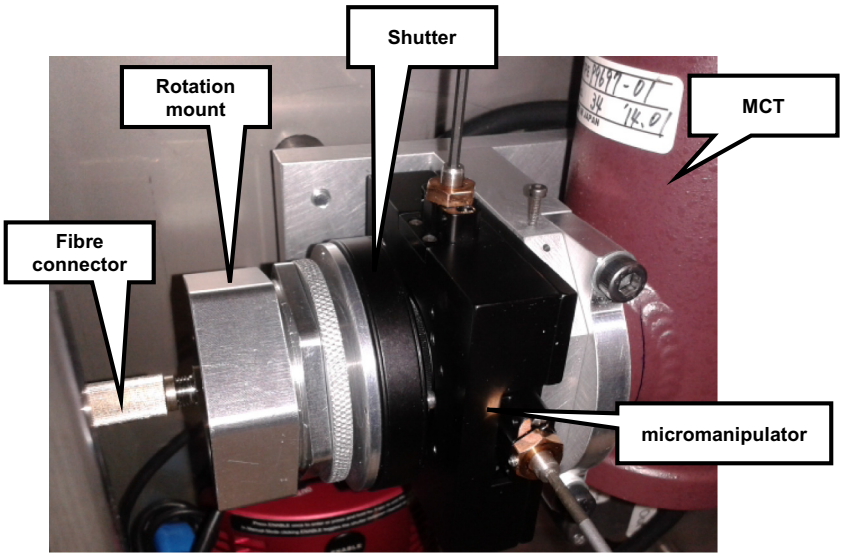

Fig. 15. Assembly of the MCT-detector in the box with optical coupler and shutter.

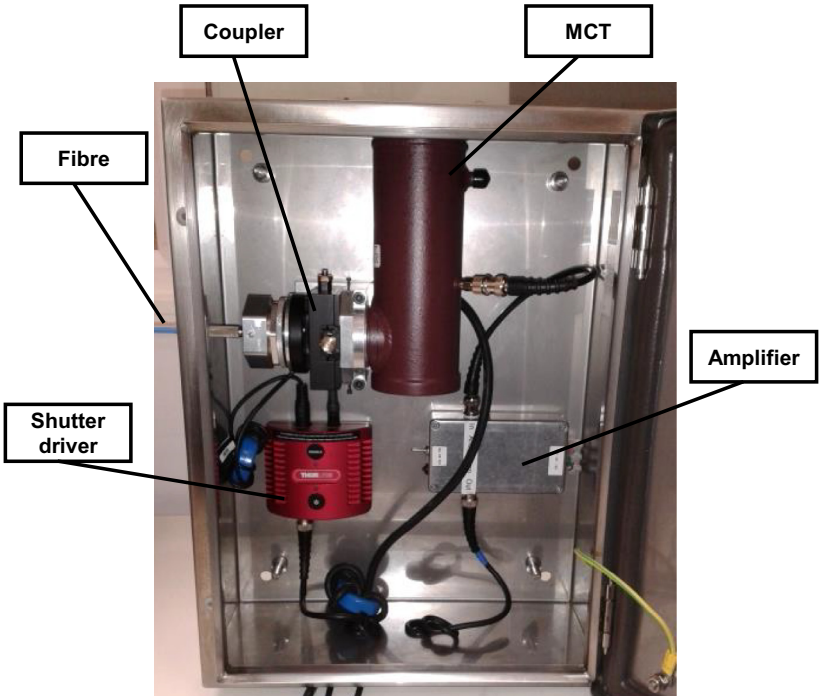

Fig. 16. Box which serves as housing of the detector and the electronics.

through the filter (Fig. 15). A shutter is placed in front of the filter which can be closed and opened in order to allow a calibration of the dark signal and a measurement of the radiation emitted by the TBC. The open box with the detector, the shutter driver and the amplifier is shown in Fig. 16.

Initial test measurements of the developed prototype LWIR-pyrometer setup have been made at the Siemens BTF. For this purpose the lance has been traversed into the flow path of a front turbine stage during engine operation and the detected radiation has been recorded. The measured intensity was then correlated with the temperature of the surface of the TBC which is applied on the turbine blades. This has been done using the emittance of the TBC, the temperature of the surrounding, the transmittance of the hot gas, the dark signal and the calibration curve of the LWIR-pyrometer. The calibration curve had been determined before the turbine measurement using a black-body radiator as reference with known temperature and unity emittance [20]. The resulting temperature signal is plotted in Fig. 17 for 10 turbine blades and in Fig. 18 for 2 turbine blades in arbitrary units for visualising the typical temperature profile. This profile is in good agree-

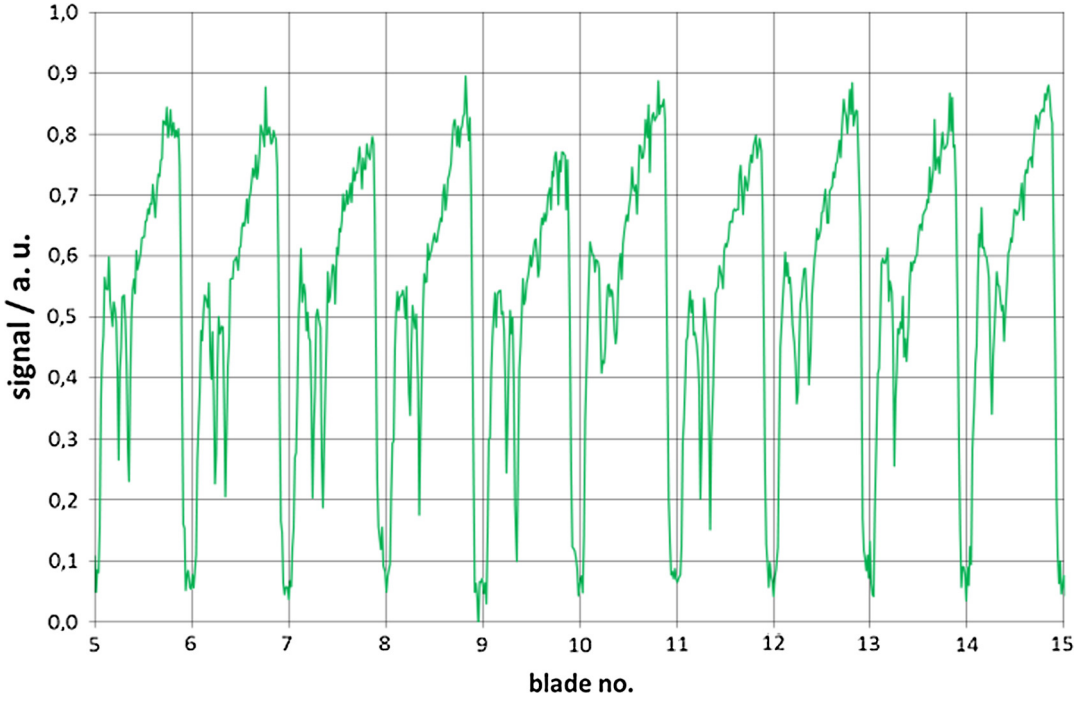

Fig. 17. Detected and analysed temperature signal of 10 turbine blades in arbitrary units.

Fig. 18. Detected and analysed temperature signal of 2 turbine blades in arbitrary units.

ment with the temperature of the TBCs. The deduced temperatures are in the expected range (see Section 4.3).

4.3. Uncertainty analysis

In general the uncertainty of the surface temperature derived from a non-contact measurement using a LWIR-pyrometer depends on several factors. In the following these factors are introduced and their influence on the developed LWIR-pyrometer is quantified. From these the total expanded standard uncertainty is determined in accordance to the procedure given in the "Guide to the expression of uncertainty in measurement (GUM)" [21].

The most relevant systematic uncertainties are given below. One important factor is the emittance of the TBC as the emitted

Table 2
The contribution of different sources of uncertainty to the uncertainty of the temperature which is determined by the developed LWIR-pyrometer is presented, together with the resulting total uncertainty.

description	sensitivity coefficient	systematic uncertainty	standard uncertainty
emittance of TBC	8 °C / %	1 %	8 °C
gaseous transmission	8 °C / %	1 %	8 °C
distance to TBC surface	1 °C / %	5 %	5 °C
correlation between emitted and reflected radiation			
radiation from optics	8 °C / %	0.5 %	4 °C
optics fouling	8 °C / %	0.5 %	4 °C
stability of detector	8 °C / %	0.5 %	4 °C
spatial resolution	15 °C / mm	0.25 mm	3.8 °C
random noise			
…			
total standard uncertainty		***k* = 1**	**14.2 °C**
total expanded standard uncertainty		***k* = 2**	**28.4 °C**

radiation not only depends on the temperature but also on the emissivity of the surface. Additionally, not only radiation from the surface, but also radiation from the surroundings which is partly reflected by the TBC is detected by the pyrometer and has to be considered when analysing the measurement signal. In this case the uncertainty is due to the uncertainty of the knowledge of the surrounding conditions (mainly the temperature of the surrounding) whereas the reflectance of the TBC is closely correlated with the emittance of the TBC in the LWIR. Also, the transmittance of the hot combustion gas between the TBC and the pyrometer lance influences the detected signal, as a part of the radiation is absorbed or scattered by the gas (plus the hot gas emits radiation at certain wavelengths). Due to blade profile, the distance between the pyrometer and the turbine blade may vary by up to 100 mm during a blade passage. This leads to an additional uncertainty of the temperature reading of the LWIR-pyrometer which has been quantified by laboratory measurements. Furthermore, the components of the LWIR-pyrometer influence the uncertainty. The optics itself emits radiation which contributes to a background signal. Moreover the optics may foul due to deposition during operation of the turbine and the detector signal may drift during measurement series as the stability of the detector is limited. Finally, the dimension of the measured area or more exactly the spatial resolution influences the results. The most important random uncertainty is the noise of the measurement signal which is among others influenced by the electronic noise. Other influencing factors, such as uncertainty of calibration and digitisation errors, are significantly lower and have been reduced to below 1 °C by optimising the calibration procedures and the electronics, respectively.

In Table 2 the influencing factors are presented, with their sensitivity on the determined temperature, their uncertainty and the resulting standard uncertainty. According to GUM [21] the total standard uncertainty for a coverage factor $k = 1$ (corresponds to a level of confidence of 68%) and the total expanded standard uncertainty for a coverage factor $k = 2$ (corresponds to a level of confidence of 95%) have been calculated. The resulting values are also presented in Table 2.

5. Conclusion

To summarise the results of this work, the partners Siemens AG, Meggitt UK, and ZAE Bayern succeeded in developing a new long wavelength infrared (LWIR) radiation thermometer for studying the surface temperature of the thermal barrier coatings (TBCs) on turbine blades. This overcomes the limitations of near infrared (NIR) radiation thermometers.

Prior to this development, the TBCs were investigated with respect to their infrared-optical properties such as emittance and transmittance. The fact that the TBCs become opaque in the LWIR and exhibit a high emittance (near unity) enables LWIR pyrometry to be feasible and reduces the measurement uncertainty due to a low influence of the hot surrounding.

Initial investigations on the transmittance and absorptance of the hot combustion gas have been performed which show a high transmittance and therefore a low influence on the LWIR pyrometry. This is very promising. Further characterisation work will be performed and the results will be published in the near future.

Finally, test measurements were performed in the laboratory as well as at the Siemens BTF which demonstrated the feasibility of LWIR pyrometry.

To support the feasibility of this method, a detailed measurement uncertainty analysis has been performed. The resulting total expanded standard uncertainty is 28.4 °C. Therefore measurements with accuracy of about 28 °C are possible when using the developed LWIR-pyrometer. Future work is planned in order to further reduce the uncertainty and to validate the results under different conditions.

Based on these results, improvements to the setup will be made, especially with respect to the signal-to-noise ratio and the sensitivity of the LWIR-pyrometer which need to be optimised. To validate these improvements further engine trials will be scheduled in the future.

Acknowledgements

This work was supported by the European Community's Seventh Framework Programme under grant agreement number 314061 within the EU project "Sensors Towards Advanced Monitoring and Control of Gas Turbine Engines (acronym STARGATE)".

References

[1] D.R. Clarke, M. Oechsner, N.P. Padture, Thermal-barrier coatings for more efficient gas-turbine engines, MRS Bull. 37 (2012) 891–898.
[2] C.G. Levi, Emerging materials and processes for thermal barrier systems, Curr. Opin. Solid State Mater. Sci. 8 (2004) 77–91.
[3] T. John Ajoko, Performance monitoring of industrial gas turbine, Int. J. Eng. Sci. Invent. 3 (2014) 62–68.
[4] F. Bernhard, Technische Temperaturmessung, Springer Verlag, Berlin, 2004.
[5] L.K. Matthews, R. Viskanta, F.P. Incropera, Combined conduction and radiation heat transfer in porous materials heated by intense solar radiation, J. Sol. Energy Eng. 107 (1985) 29–34.
[6] T. Makino, T. Kunitomo, I. Sakai, H. Kinoshita, Thermal radiation properties of ceramic materials, Heat Transf. – Jpn. Res. 13 (1984) 33–50.
[7] J. Manara, M. Arduini-Schuster, H.-J. Rätzer-Scheibe, U. Schulz, Infrared-optical properties and heat transfer coefficients of semitransparent thermal barrier coatings, Surf. Coat. Technol. 203 (2009) 1059–1068.
[8] J. Manara, M. Arduini-Schuster, M.H. Keller, Infrared-optical characteristics of ceramics at elevated temperatures, Infrared Phys. Technol. 54 (2011) 395–402.
[9] C.G. Levi, J.W. Hutchinson, M.-H. Vidal-Sétif, C.A. Johnson, Environmental degradation of thermal-barrier coatings by molten deposits, MRS Bull. 37 (2012) 932–941.
[10] L. Hanssen, Integrating-sphere system and method for absolute measurement of transmittance, reflectance, and absorptance of specular samples, Appl. Opt. 40 (2001) 3196–3204.
[11] J. Manara, M. Arduini-Schuster, L. Hanssen, Infrared-optical intercomparison measurements for evaluating the accuracies of the achieved results, High Temp. – High Press. 38 (2009) 259–276.
[12] J. Manara, R. Caps, H.-P. Ebert, F. Hemberger, J. Fricke, A. Seidl, Infrared optical properties of semitransparent pyrolytic boron nitride (pBN), High Temp. – High Press. 34 (2002) 65–72.
[13] J. Manara, R. Brandt, J. Kuhn, J. Fricke, T. Krell, U. Schulz, M. Peters, W.A. Kaysser, Emittance of Y_2O_3 stabilised ZrO_2 thermal barrier coatings prepared by electron beam physical vapour deposition, High Temp. – High Press. 32 (2000) 361–368.
[14] M. Rydzek, T. Stark, M. Arduini-Schuster, J. Manara, Newly designed apparatus for measuring the angular dependent surface emittance in a wide wavelength range and at elevated temperatures up to 1400 °C, JPCS 395 (2012) 012152.
[15] M.-P. Bacos, J.-M. Dorvaux, O. Lavigne, R. Mevrel, M. Poulain, C. Rio, M.-H. Vidal Setif, Performance and degradation mechanism of thermal barrier coatings for turbine blades: a review of onera activities, Therm. Barrier Coat. Turb. Blades 3 (2011) 1–11.
[16] P.M. Borom, C.A. Johnson, L.A. Peluso, Role of environmental deposits and operating surface temperature in spallation of air plasma sprayed thermal barrier coatings, Surf. Coat. Technol. 86–97 (1996) 116–126.
[17] J. Manara, M. Keller, D. Kraus, M. Arduini-Schuster, Determining the transmittance and emittance of transparent and semitransparent materials at elevated temperatures, in: G.G.M. Stoffels, T.H. van der Meer, A.A. van Steenhoven (Eds.), Proceedings 5th European Thermal-Sciences Conference, 20.05.2008, Eindhoven, Netherlands, 2008, ISBN 978-90-386-1274-4.
[18] H. Günzler, H.-U. Gremlich, IR Spectroscopy: An Introduction, Wiley-VHC, Weinheim, 2002.
[19] B. Rousseau, J.F. Brun, D. De Sousa Meneses, P. Echegut, Temperature measurement: christiansen wavelength and blackbody reference, Int. J. Thermophys. 26 (2005) 1277–1286.
[20] J. Hartmann, High-temperature measurement techniques for the application in photometry radiometry and thermometry, Phys. Rep. 469 (2009) 205–269.
[21] JCGM 100:2008 GUM 1995 with Minor Corrections: Evaluation of Measurement Data – Guide to the Expression of Uncertainty in Measurement, first ed., September 2008.